A LOWER TROPHIC ECOSYSTEM MODEL INCLUDING IRON EFFECT IN THE OKHOTSK SEA

OKUNISHI T.[1] AND KISHI M. J.[2]

[1] *Graduate School of Engineering, Hokkaido University*

[2] *Graduate School of Fisheries Sciences, Hokkaido University*

ABSTRACT

We applied a three dimensional ecosystem - physical coupled model including iron effect to the Okhotsk Sea. In order to clarify the sources of iron, four dissolved iron compartments, based on the sources of supply, were added to Kawamiya et al. (1995)'s model (KKYS) to create our ecosystem model (KKYS-Fe). We hypothesized that four processes supply iron to sea water: atmospheric loadings from Northeastern Asia, input from the Amur River, dissolution from sediments and regeneration by zooplankton and bacteria. We simulated 1year, from 1 January, 2001 to 31 December, 2001, using both KKYS-Fe and KKYS. KKYS could not reproduce the surface nitrate distribution after the spring bloom, whereas KKYS-Fe agreed well with observations in the northwestern Pacific because it includes iron limitation of phytoplankton growth. During spring bloom, the main source of iron at the sea surface is from the atmosphere. The contribution of riverine iron to total iron utilized for primary production is small in the Okhotsk Sea. Atmospheric deposition, iron flux from sediment and regeneration of iron in the water column play an important role in maintenance of high primary production in the Okhotsk Sea.

MODEL DESCRIPTION

Material flows in our ecosystem model are shown in Fig. 1. This model is based on Kawamiya et al. (1995) (referred to as KKYS hereinafter), which is a nitrogen-based model with 6 compartments (phytoplankton; Phy, zooplankton; Zoo, nitrate; NO_3, ammonium; NH_4, Detritus; D, dissolved organic matter; DOM). Four iron compartments were added, separated according to source as shown in Fig.1 (KKYS-Fe), in order to clarify the sources of iron. We assumed that the process of dissolved iron-supply to the Okhotsk Sea are: 1) atmospheric loadings from Northeastern Asia (FE_{AIR}), 2) riverine input from the Amur River (FE_{RIV}), 3) dissolution from sediments (FE_{SED}), and 4) biological regeneration by zooplankton and bacteria (FE_{BIO}). Dissolved iron fraction the source of which cannot be identified is also included in this compartment (FE_{BIO}). We assumed that all dissolved iron is bioavailable and that particulate iron is not bioavailable (and therefore neglected in the model). We also suppose that the phytoplankton and zooplankton have the same iron/nitrogen ratio 0.044 in [nmol : μmol], assuming a carbon/nitrogen ratio of 106: 16 for phytoplankton, based on

Gregg (2002) and Gregg et al. (2003). We used the same iron/nitrogen ratio in the other compartments (Detritus, DOM).

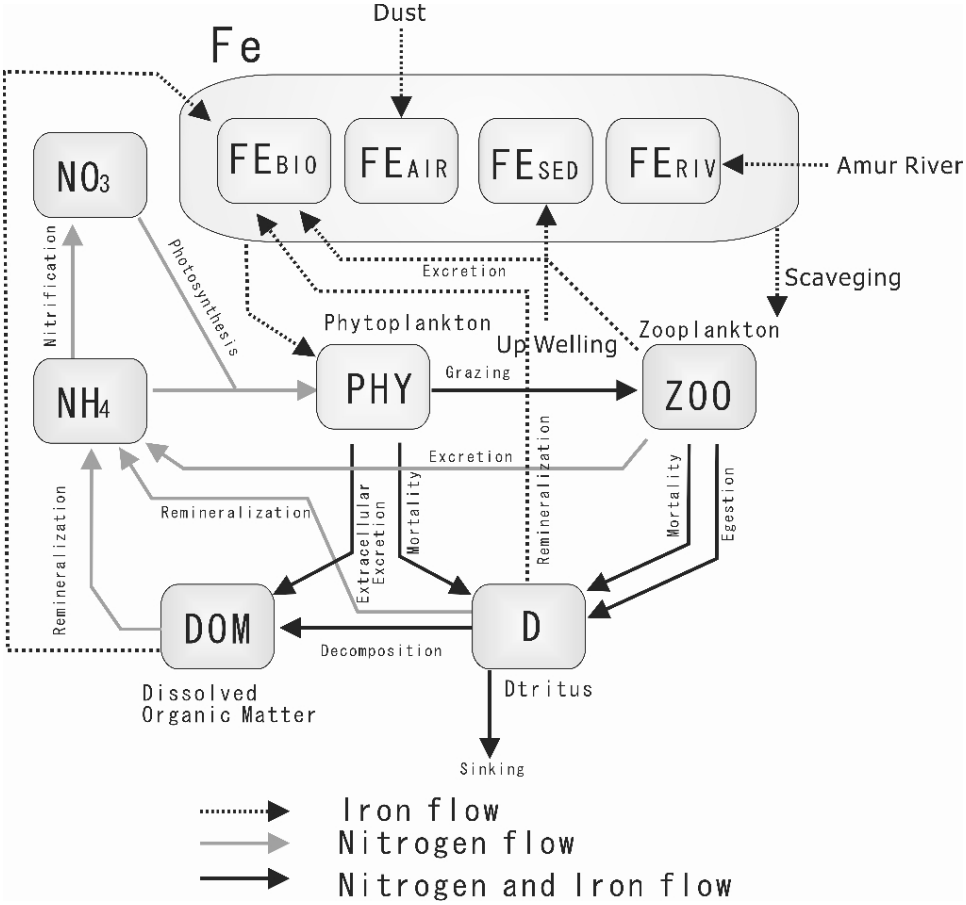

Figure 1: A schematic view of ecosystem model

FORMULATION OF ECOLOGICAL PROCESSES

Time evolution of each compartment is described as follows;

$$\frac{\partial C_i}{\partial t} = -v \cdot \nabla C_i + \nabla(K \nabla C) + (biological term) \quad (1)$$

where C_i is arbitrary compartments, v current velocity, and K diffusion tensor. The mathematical formulations for the nitrogen flow followed those of Kawamiya et al., (1995). The new and modified formulations are as follows;

Photosynthesis: Michaelis-Menten formula was adopted for iron uptake by phytoplankton. Noiri et al., (2005) reported that the half-saturation constant for iron is 0.59 nM (at 5 °C) and 0.58 (at 8 °C) for photosynthesis (>10 micro m size fraction) in the western subarctic Pacific. In this model, 0.58 was used for (K_{FFe}). Ammonium inhibition was taken into account (Wroblewski, 1977) in the original KKYS. We modified the half saturation constants (Moore et al., 2002) to account for the increased preference for ammonium under iron limitation. The half-saturation constant for nitrate uptake was increased to as much as 150% of its original value (Eqs.8 and 9) with increasing iron stress. Likewise, the half-saturation constant for

ammonium was decreased to 50% of its original value with increasing iron stress (Eqs. 8 and 9).

$$(\text{Photosynthesis}) = GPP(Phy, NH_4, NO_3, Fe, T, I) = V_{\max}\{\min(LIMITN, LIMETFe)\} \times \exp(kT)\frac{I}{I_{opt}}\exp\left(1-\frac{I}{I_{opt}}\right)Phy \quad (2)$$

$$I = I_0 \exp(-\Lambda|z|) \quad (3)$$

$$\Lambda = \alpha_1 + \alpha_2 \times Phy \quad (4)$$

$$LIMITN = \left\{\frac{NO_3}{NO_3 + K_{NO3}}\right\} \times \exp(-\Psi NH_4) + \frac{NH_4}{NH_4 + K_{NH4}} \quad (5)$$

$$LIMITFe = \frac{TFe}{FFe + K_{Fe}} \quad (6)$$

$$TFe = FE_{AIR} + FE_{RIV} + FE_{SED} + FE_{BIO} \quad (7)$$

$$TFe < K_{Fe}: \begin{matrix} K_{NO3} = K_{NO3} \\ K_{NH4} = K_{NH4} \end{matrix} \quad (8)$$

$$TFe \geq K_{Fe}: \begin{matrix} K_{NO3} = K_{NO3} \times 1.5 \\ K_{NH4} = K_{NH4} \times 0.5 \end{matrix} \quad (9)$$

where T is temperature, z is depth, positive upward (zero at the sea surface), I light intensity, I_{opt} optimum light intensity, I_0 photosynthetically active radiation (PAR) at the sea surface, Λ the light dissipation coefficient, and TFe total dissolved iron concentration. Notation for parameters is given in Table 1 with their values. Parameters used to describe other processes are also given in this table. Here, the fraction of iron uptake from each compartment (FE_{AIR}, FE_{RIV}, FE_{SED}, FE_{BIO}) is defined as follows to simplify later discussion.

$$RAFE = \frac{FE_{AIR}}{TFe},\ RRFE = \frac{FE_{RIV}}{TFe},\ RSFE = \frac{FE_{SED}}{TFe},\ RBFE = \frac{FE_{BIO}}{TFe} \quad (10)$$

Atmospheric iron flux: The main source of dissolved iron to surface water in most areas of the open ocean is dust deposited at the sea surface (Duce and Tindale, 1991). Atmospheric iron flux is added to the first layer of the model at each time step of the ecological calculation. Duce and Tindale (1991) estimated global atmospheric iron flux based on Donaghay et al. (1991), assuming that 3.5% (w/w) of the atmospheric dust contributes as iron flux. Fung et al., (2000) estimated an iron budget for the upper ocean using solubilities of 1% and 10 %. We assumed that 1 % of atmospheric iron is dissolved into the dissolved iron pool. We considered seasonal variation of iron flux by using the Gaussian function after Littmann (1991) .

Iron flux from the Amur River: The Amur River is one of the largest rivers in East and North-East Asia. It supplies significant freshwater to the Okhotsk Sea, is 4440 km long, and drains an area of 1,885,000 km^2. The minimum discharge is about 1,000 m^3 s^{-1} in March. Its discharge starts to increase in April, reaches a maximum (up to 200,000 m^3 s^{-1}) in September, gradually decreases in October, December, and then remains near the minimum level. The major part of the drainage area is underlain by boreal forest, mixed forest and swamps. Dissolved iron concentration of the Amur River is 0.56($\pm$0.17) mg L^{-1} (Shibata, 2005). It is well known that salinity plays important role in the aggregation process of dissolved iron at an estuary. Colloidal iron definitely plays a leading role in controlling the iron behavior in the

mixing process at estuaries, and its flocculation is responsible to the removal of the dissolved iron. Sholkovitz (1976) pointed out that 100% of riverine iron is precipitated by flocculation under the influence of oceanic salinities. On the other hand, about 93% of dissolved iron in Lena River was removed at the mouth of the Laptev Sea (Guieu et al, 1996). Predue *et al*. (1976) found a strong correlation between dissolved organic matter (fulvic acid) and iron concentration in natural waters. Figures *et al*. (1978) reported that organically-bound iron in river water can remain without sinking and is diffused into coastal water. Now, we assumed that 99 % of the riverine iron is lost in the estuary, so that 1 % of the riverine iron was the fluvial iron, and the dissolved iron concentration supplied to the Okhotsk Sea from the Amur River is 100 nM.

PHYSICAL MODEL

POM (Blumberg and Mellor, 1987; Galperina and Mellor, 1990) was used for the ocean model. This model is a three-dimensional, free surface, ocean model with a second moment turbulence closer scheme (Mellor and Yamada, 1982) to provide vertical mixing coefficients. The model domain extends from 34°N to 63°N and from 127°E to 166°E, which does not include the Japan Sea. The Soya and Tsugaru straits are closed, and grids shallower than 30 m depth are masked. The horizontal grid scale is 1/6°. POM uses a sigma coordinate system in the vertical. In deep area, sigma coordinate system cannot resolve adequately near the surface, because the layer thickness becomes large. Therefore, the fixed z-levels coordinate system is used for upper 10 levels, while lower 10 levels are sigma levels.

***Sea ice effect*:** In this study we used the NCAR Climate System Sea ICE Model (Bettge et al., 1996). The momentum dynamics in the above model are based on the model by Flato and Hibler (1992). The thermodynamics of ice growth and melting processes are taken from Semtner (1976), Parkinson and Washington (1979), Harvey (1988), and Pollard and Thompson (1994). Sea ice affects the momentum in the ocean model and the light under ice in the ecological model. The estimated momentum flux and light intensity under ice are as follows.

(Momentum flux under sea ice); Under the existence of sea ice, there is a momentum flux from the atmosphere to the surface water, via the sea ice. Momentum flux in the ocean model is $\tau_x = \tau_a + \tau_i$, τ_a is the moment flux from the atmosphere to surface water, τ_i is the moment flux from sea ice to surface water. Momentum flux from the atmosphere to surface water is described as: $\tau_a = \rho C_d W_x \sqrt{W_x^{\,2} + W_y^{\,2}}\left(1 - IC/100\right)$ (23) where, ρ is sea water density, C_d is drug coefficient W_x is zonal wind speed, W_y is meridional wind speed, and IC is sea ice concentration in per cent. Momentum flux from the sea ice to surface water is described as**:** $\tau_i = \rho_w C_{Dw} |u_i - u_w| (u_i - u_w)(IC/100)$ (24) where ρ_w is surface water density, C_{DW} is drug coefficient ($4*10^{-3}$), u_i is sea ice velocity, u_w is surface water velocity.

(Light condition under sea ice): The incident light strength under sea ice (I_d) is described as follows;

$$I_d = I_0(1-r)e^{-\alpha \cdot d} \times (1 - IC/100) \quad (25)$$

where, I_0 is the incident light strength at the surface of sea ice, r is the reflectivity at the sea ice surface, d is thickness of sea ice and α is the extinction coefficient of sea ice. Gilgert and Buntzen (1984) reported that the extinction coefficient in sea ice of 10 cm thickness was 0.025 cm^{-1}. We used this value. Ishikawa et al. (2003) reported the value of 0.04 as the reflectivity at the sea ice surface, and this value is used in our model. The thickness of sea ice is estimated by the sea ice model described above.

MODEL RUN

The simulation was conducted for one year from 1 January, 2001 to 31 December, 2001. In 2001 a large ice-coverage was observed in the Okhotsk Sea; maximum ice area was about 99% in the winter. The momentum fluxes are calculated with the zonal and meridional wind speeds from National Centers for Environmental Prediction and National Center for Atmospheric Research (NCEP / NCAR) reanalysis data (Kalnay et al., 1996). The model can reproduce the seasonal prevalence of sea ice in the Okhotsk Sea in 2001.

RESULTS AND DISCUSSION

Nitrate, Chl-a and iron concentration

Saitoh et al., (1996) showed that the spring bloom usually occurred between April and May in the Okhotsk Sea based on the monthly coastal zone color scanner (CZCS)-chlorophyll (Chl) imagery from 1978 until 1986. Figure 3 shows the time-dependent features of Chl-a concentrations and nitrate concentrations in the surface layer (0-20 m) at five stations (see Fig.2).

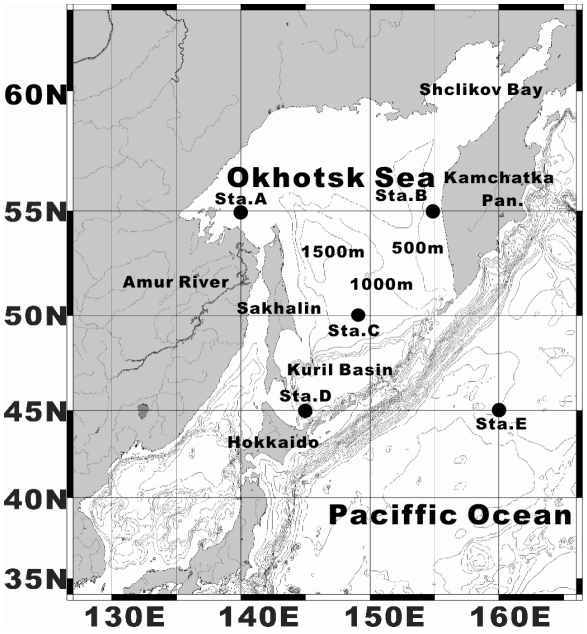

Figure 2: Staions for output of the model

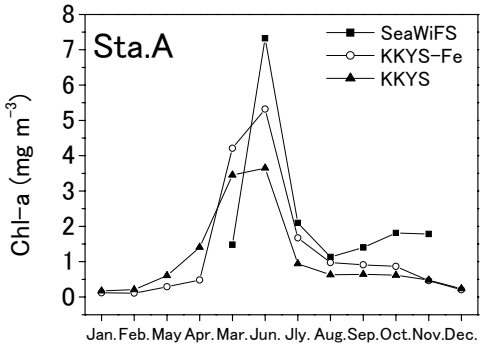
Sta.A
SeaWiFS
KKYS-Fe
KKYS
Chl-a (mg m^{-3})
Jan. Feb. May Apr. Mar. Jun. Jly. Aug. Sep. Oct. Nov. Dec.

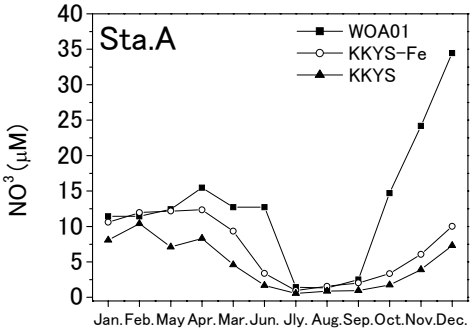
Sta.A
WOA01
KKYS-Fe
KKYS
NO^3 (μM)
Jan. Feb. May Apr. Mar. Jun. Jly. Aug. Sep. Oct. Nov. Dec.

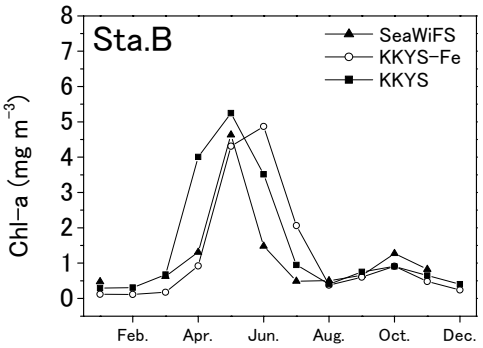
Sta.B
SeaWiFS
KKYS-Fe
KKYS
Chl-a (mg m^{-3})
Feb. Apr. Jun. Aug. Oct. Dec.

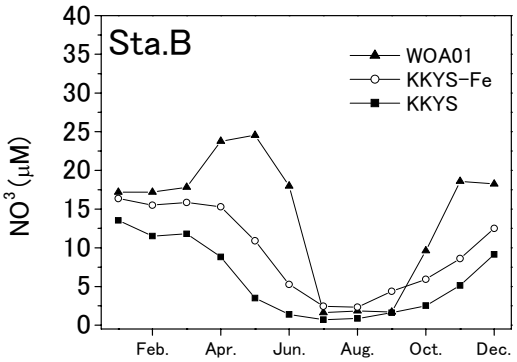
Sta.B
WOA01
KKYS-Fe
KKYS
NO^3 (μM)
Feb. Apr. Jun. Aug. Oct. Dec.

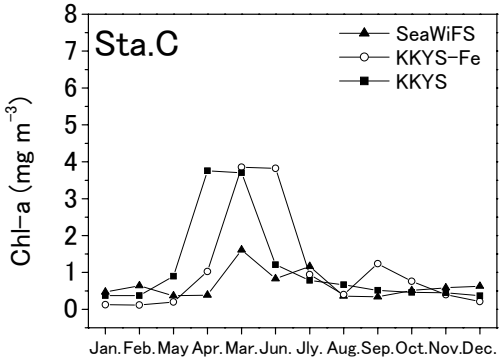
Sta.C
SeaWiFS
KKYS-Fe
KKYS
Chl-a (mg m^{-3})
Jan. Feb. May Apr. Mar. Jun. Jly. Aug. Sep. Oct. Nov. Dec.

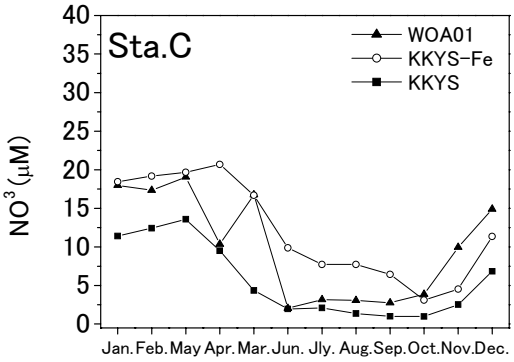
Sta.C
WOA01
KKYS-Fe
KKYS
NO^3 (μM)
Jan. Feb. May Apr. Mar. Jun. Jly. Aug. Sep. Oct. Nov. Dec.

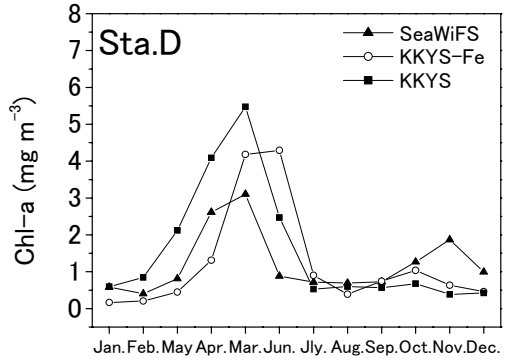
Sta.D
SeaWiFS
KKYS-Fe
KKYS
Chl-a (mg m^{-3})
Jan. Feb. May Apr. Mar. Jun. Jly. Aug. Sep. Oct. Nov. Dec.

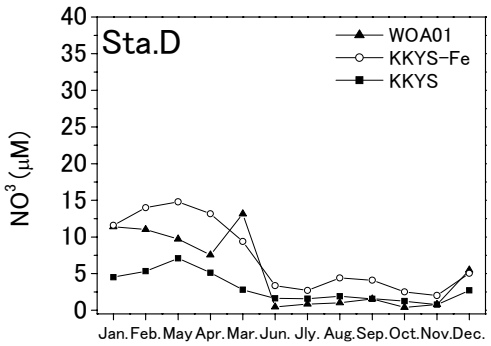
Sta.D
WOA01
KKYS-Fe
KKYS
NO^3 (μM)
Jan. Feb. May Apr. Mar. Jun. Jly. Aug. Sep. Oct. Nov. Dec.

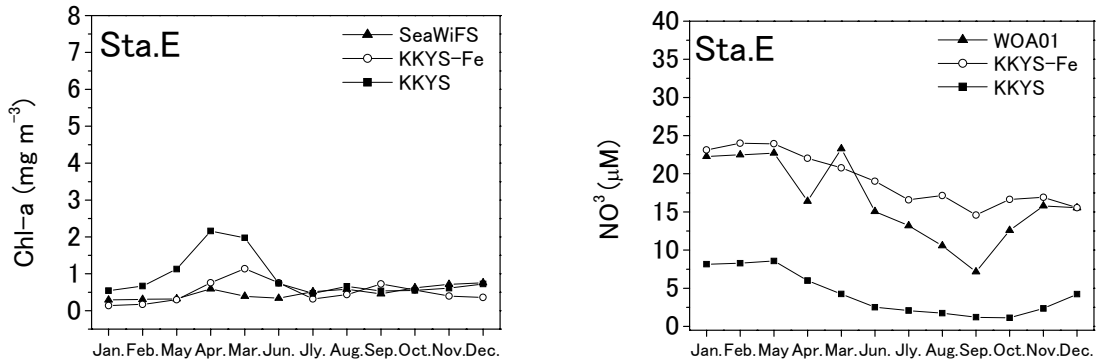

Figure 3: Time-dependent features of Chl-a and nitrate concentrations at the surface layer (20 m) in five study points shown Fig. 1. Left figures show Chl-a concentrations from SeaWiFS data, KKYS-Fe, KKYS. Right figures show nitrate concentrations from World Ocean Atlas data, KKYS-Fe, KKYS

Chl-a concentrations both by KKYS-Fe and by KKYS coincide to the time variation of SeaWiFS features in all stations. But the spring bloom peak by KKYS-Fe occurs slightly later than in SeaWiFS except for Sta. A. Nitrate concentrations by KKYS-Fe and KKYS also agree with the seasonal variation of WOA01's nitrate concentrations in all stations except at Sta.E. At Sta.E (northwestern Pacific) nitrate concentration by KKYS is underestimated, and Chl-a concentration is overestimated during the spring. Fig 4 shows sea surface nitrate distribution simulated by KKYS and KKYS-Fe together with the observed value from WOA 2001 in March. In March, before the spring bloom, results of KKYS-Fe agree well with the observation, but those of KKYS do not in the northwestern Pacific. As shown in Fig. 4 (a, b), nitrate concentration is relatively high in the northwestern Pacific. After the spring boom (July), the sea surface nitrate is depleted in almost all areas of the Okhotsk Sea and remain more than 5nM in the northwestern Pacific (Fig. 5a). KKYS-Fe' (Fig. 5b) shows almost the same features as the WOA 2001 data in both the Okhotsk Sea and the northwestern Pacific. On the other hand, KKYS can never reproduce this surface nitrate distribution either-(Fig. 5c), but the sea surface nitrate is depleted in almost whole areas.

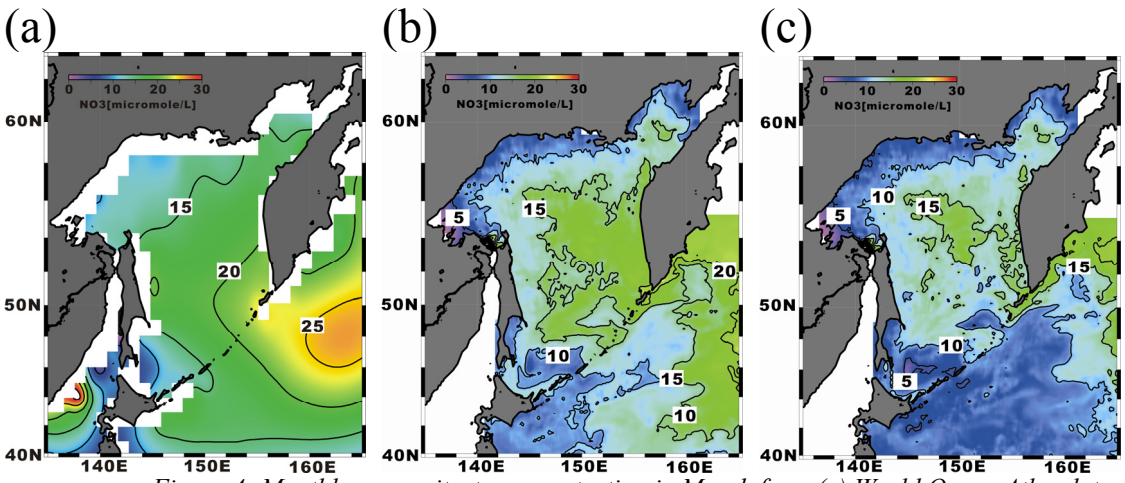

Figure 4: Monthly mean nitrate concentration in March from (a) World Ocean Atlas data, (b) KKYS-Fe and (c) KKYS in surface water (averaged from 0m to 20m).

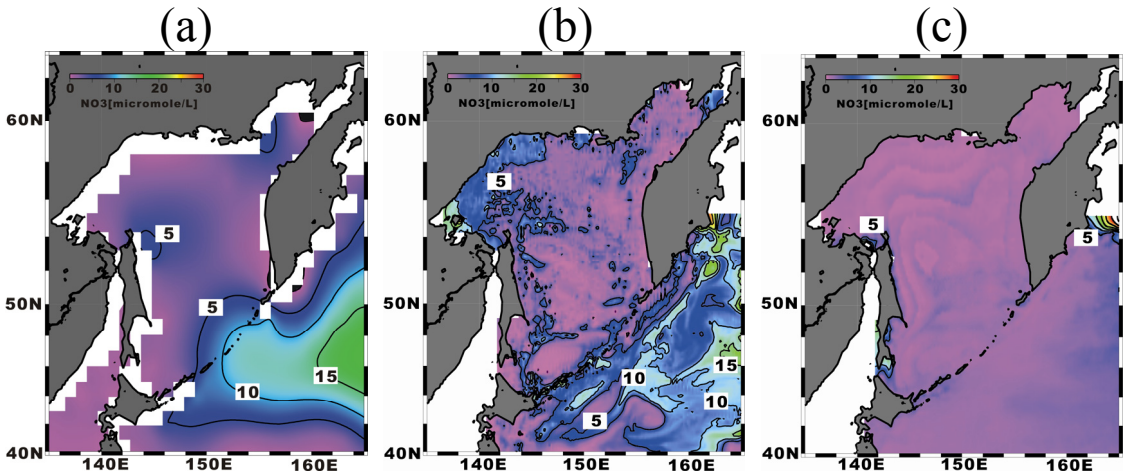

Figure 5: Same as Fig.4 but for July.

CONCLUSION

This study is the first to examine the iron sources in the Okhotsk Sea by using an ecosystem model including iron effect. Our results suggest that atmospheric deposition, iron flux from sediment and biologically regeneration of iron in water column play an important role in maintaining high primary production in the Okhotsk Sea. Contribution of atmospheric deposition of iron for primary production during the spring bloom in the Okhotsk Sea is extremely large, and biologically regenerated iron (FE_{BIO}) is as well through the year.

Table 1. The ecological model parameters values.

V_{max}	Max Photosynthesis Rate at 0℃	0.5	/day
k	k Temperature Coefficient for Photosynthetic Rate	0.063	/℃
I_{opt}	Optimum Light Intensity	80	W/m^2
K_I	Half saturation coefficient for light intensity.	0.0336	W/m^2
α_1	Light Dissipation Coefficient of Sea Water	0.035	/m
α_2	Self Shading Coefficient	0.0281	l/μmolN m
Ψ	Ammonium Inhibition Coefficient	1.5	l/μmol
K_{NO3}	Half Saturation Coefficient for Nitrate	3.0	μmol/l
K_{NH4}	Half Saturation Coefficient for Ammonium	0.5	μmol/l
K_{Fe}	Half Saturation Coefficient for iron	0.58	nmol/l
FENR	Fe/N Ratio to Phytoplankton	0.044	nmol/μmol
M_{P0}	Phytoplankton Mortality Rate at 0℃	0.0281	l/μmolN day
k_{MP}	Temperature Coefficient for Phytoplankton Mortality	0.069	/℃
M_{Z0}	Zooplankton Mortality Rate at 0℃	0.0585	l/μmolN day
k_{MZ}	Temperature Coefficient for Zooplankton Mortality	0.0693	/℃
γ	Ratio of Extracelluler Excretion to Photosynthesis	0.135	-
GR_{max}	Max Grazing Rate at 0℃	0.30	/day
k_g	Temperature Coefficient for Grazing	0.0693	/℃
λ	Ivlev Constant	1.4	l/μmolN
Chl*	Threshold Value for Grazing	0.043	μmolN/l
α	Assimilation Efficiency of Zooplankton	0.7	-
β	Growth Efficiency of Zooplankton	0.3	-
V_{PI0}	Dtritus Decomposition Rate at 0° C (to Inorganic Nitrogen)	0.030	/℃
V_{PIT}	Temperature Coefficient for Dtritus Decomposition (to Inorganic Nitrogen)	0.0693	/day
V_{PD0}	Dtritus Decomposition Rate at 0° C (to DON)	0.030	/℃
V_{PDT}	VPDT Temperature Coefficient for Dtritus Decomposition (to DON)	0.0693	/day
V_{DI0}	VDI0 DON Decomposition Rate at 0° C	0.030	/℃
V_{DIT}	VDIT Temperature Coefficient for DON Decomposition	0.0693	/day
k_{N0}	kN0 Nitrification Rate at 0°C	0.030	/℃
k_{NT}	kNT Temperature Coefficient for Nitrification	0.0693	/day
S	Sinking velocity of Dtritus	10	m/day

REFERENCES

Bettge T. W., J. W. Weatherly, W. M. Washington, D. Pollard, B. P. Briegleb, W. G. Strand Jr., 1996. The NCAR CSM Sea Ice Model, NCAR Technical Note, TN-425+STR, National Center for Atmospheric Research, Boulder, Colorado, 30 pp.

Blumberg, A. F., Mellor G. L., 1987. A description of a three-dimensional coastal ocean circulation model. In: Heaps, N.S., Editor, Three-dimensional Coastal Ocean Models Coastal and Estuarine Sciences vol. 4, AGU, Washington, 1–16

Donaghay, P.L., Liss, P.S., Duce, R.A., Kester, D.R., Hanson, A.K., Villareal, T., Tindale, N.W., Gifford, D.J., 1991. The role of episodic atmospheric nutrient inputs in the chemical and biological dynamics of oceanic ecosystems. Oceanography, 4, 2, 62-70.

Duce, R.A., Tindale, N.W.,, 1991. Atmospheric transport of iron and its deposition in the ocean. Limnology and Oceanography, 36, 17155 - 1726

Figures, G., Martin, J. M., Meybeck, M., 1978. Iron behavior in the Zaire Estuary. Netherlands Journal of Sea Research 12, 329-337.

Flato, G. M. and W. D. Hibler, 1992. Modeling pack ice as cavitating fluid. J. Phys. Oceanogr. 22, 626-651.

Fung, I.Y., Meyn, S.K., Tegen, I., Doney, S.C., John, J.G., Bishop, J.K.B., 2000. Iron supply and demand in the upper ocean. Global Biogeochemical Cycles, 14, 281–291

Galperina, B., Mellor, G. L., 1990. A time-dependent, three-dimensional model of the Delaware Bay and River system. Part 1: Description of the model and tidal analysis. Estuarine, Coastal and Shelf Science, 31, 231-253.

Gilgert, G. D., Buntzen, R. R., 1984. In-situ measurements of the optical properties of arctic sea ice. SPIE Vol.637 Ocean Optics 8, 232-263

Guieu, C., Huang, W-W., Martin, J-M., Yong, Y-Y., 1996. Outflow of trace metal into the Laptev Sea by the Lena River. Marine Chemistry, 53, 255-267

Harvey, L.D.D., 1988. Development of a sea ice model for use in zonally averaged energy balance climate models. J. Clim. 1, 1221-1238.

Ishikawa,N., Takizawa,A., Kawamura,T., Shirasawa,K. and Lepparanta,M., 2003. Changes of the radiation property with sea ice growth in Saroma Lagoon and the Baltic Sea. Report Series in Geophysics, 46, 147-160

Kalnay, E., Kanamitsu, M., Kistler, R., Collins, W., Deaven, D., Gandin, L., et al., 1996. The NCEP/NCAR 40-Year Reanalysis Project, Bull. Am. Meteorol. Soc., 77, 3), pp. 437–470

Kawamiya, M., Kishi, M. J., Yamanaka, Y., Suginohara, N., 1995. An ecological-physical coupled model applied to Station Papa. Journal of Oceanography, 51, 635-664

Littmann, T., 1991. Dust storm frequency in Asia: Climatic control and variability, Int. J. Climatol., 11, 393-412

Mellor, G. L., Yamada, T., 1982. Development of a turbulence closure model for geophysical fluid problems. Rev. Geophys. Space Phys., 20, 851-875

Moore J. K., Doneya, S. C., Kleypasa, J. A., Gloverb, D. M., Fungc, I. Y., 2002. An intermediate complexity marine ecosystem model for the global domain. Deep-Sea Research II, 49, 403–462

Noiri, Y., Kudo, I., Kiyosawa, H., Nishioka, J., Tsuda, A., 2005. Iron and temperature, two factors inXuencing phytoplankton species composition in the westerns subarctic PaciWc Ocean. Progress in Oceanography, 64, 149-166

Parkinson, C. L. and W. M. Washington, 1979. A large-scale numerical model of sea ice. J. Geophys. Res. 84, 311-337.

Pollard, D., and S. L. Thompson, 1994. Sea-ice dynamics and CO_2 sensitivity in a global climate model. Atmosphere-Ocean 32, 449-467.

Predue, E.H., Beck, K. C. and Reuter, J. H., 1976. Organic complexes of iron and aluminum in natural waters. Nature 260, 418-420.

Saitoh, S., Kishino, M., Kiyofuji, H., Taguchi S., Takahashi, M., 1996. Seasonal variability of phytoplankton pigment concentration in the Okhotsk Sea. Journal of the Remote Sensing Society of Japan, 16, 86-92

Semtner, A. J., 1976. A model for the thermodynamic growth of sea ice in numerical investigations of climate. J. Phys. Oceanogr. 6, 379-389

Sholkovitz, E.R., 1976. Flocculation of dissolved organic and inorganic matter during the mixing of river water and seawater. Geochimica et Cosmochimica Acta, 40, 831-845.

Shibata, H., 2005. Process of iron transport from terrestrial ecosystem to river: - Preliminary analysis of spatial and temporal patterns of iron concentration in Amur River -, Proceeding of the Inter national Kyoto Symposium 2005, Report on Amur-Okhotsk Project No.3, December 2005, 97-104.

Wroblewski, J. S., 1977. A model of phytoplankton plume formation during Oregon upwelling. J. Mar. Res., 35, 357–394